Article:
Mias-Lucquin, D., Dos Santos Morais, R., Chéron, A. et al. (2020) How the central domain of dystrophin acts to bridge F-actin to sarcolemmal lipids. Journal of Structural Biology, 209 (1). 107411. ISSN: 1047-8477

https://doi.org/10.1016/j.jsb.2019.107411

Journal of Structural Biology 209 (2020) 107411

Contents lists available at ScienceDirect

Journal of Structural Biology

journal homepage: www.elsevier.com/locate/yjsbi

How the central domain of dystrophin acts to bridge F-actin to sarcolemmal lipids

Dominique Mias-Lucquin[a,1], Raphael Dos Santos Morais[a,b,c,1,2], Angélique Chéron[a], Mélanie Lagarrigue[d,e], Steve J. Winder[f], Thomas Chenuel[a], Javier Pérez[c], Marie-Sousai Appavou[g], Anne Martel[h], Guillaume Alviset[a], Elisabeth Le Rumeur[a], Sophie Combet[b], Jean-François Hubert[a], Olivier Delalande[a,*]

[a] Univ Rennes, CNRS, IGDR – UMR6290, F-35000 Rennes, France
[b] Laboratoire Léon-Brillouin, UMR 12 CEA-CNRS, Université Paris-Saclay, CEA-Saclay, F-91191 Gif-sur-Yvette CEDEX, France
[c] SWING Beamline, Synchrotron SOLEIL, L'Orme des Merisiers, BP 48, Saint-Aubin, F-91192 Gif-sur-Yvette, France
[d] Univ Rennes, Inserm, EHESP, Irset (Institut de recherche en santé, environnement et travail) UMR_S 1085, F-35000 Rennes, France
[e] Protim, Univ Rennes, F-35000 Rennes, France
[f] Department of Biomedical Science, University of Sheffield, Sheffield, S10 2TN UK
[g] Jülich Centre for Neutron Science (JCNS) at Heinz Maier-Leibnitz Zentrum (MLZ), Forschungszentrum Jülich GmbH, Lichtenbergstr. 1, D-85748 Garching, Germany
[h] Institut Laue-Langevin, F-38042 Grenoble, France

ARTICLE INFO

Keywords:
Dystrophin
F-actin
Bicelle membrane model
Small-angle scattering
Molecular modelling
Mass spectrometry

ABSTRACT

Dystrophin is a large intracellular protein that prevents sarcolemmal ruptures by providing a mechanical link between the intracellular actin cytoskeleton and the transmembrane dystroglycan complex. Dystrophin deficiency leads to the severe muscle wasting disease Duchenne Muscular Dystrophy and the milder allelic variant, Becker Muscular Dystrophy (DMD and BMD). Previous work has shown that concomitant interaction of the actin binding domain 2 (ABD2) comprising spectrin like repeats 11 to 15 (R11-15) of the central domain of dystrophin, with both actin and membrane lipids, can greatly increase membrane stiffness. Based on a combination of SAXS and SANS measurements, mass spectrometry analysis of cross-linked complexes and interactive low-resolution simulations, we explored *in vitro* the molecular properties of dystrophin that allow the formation of ABD2-F-actin and ABD2-membrane model complexes. In dystrophin we identified two subdomains interacting with F-actin, one located in R11 and a neighbouring region in R12 and another one in R15, while a single lipid binding domain was identified at the C-terminal end of R12. Relative orientations of the dystrophin central domain with F-actin and a membrane model were obtained from docking simulation under experimental constraints. SAXS-based models were then built for an extended central subdomain from R4 to R19, including ABD2. Overall results are compatible with a potential F-actin/dystrophin/membrane lipids ternary complex. Our description of this selected part of the dystrophin associated complex bridging muscle cell membrane and cytoskeleton opens the way to a better understanding of how cell muscle scaffolding is maintained through this essential protein.

1. Introduction

Dystrophin is a large intracellular protein that contributes to support membrane stretching or bending stresses developed during muscle contraction and relaxation. It provides a mechanical link between the intracellular actin cytoskeleton and the transmembrane dystroglycan complex and thus helps prevent sarcolemmal ruptures (Campbell and Kahl, 1989) mainly by behaving as a shock absorber (Ramaswamy et al., 2011; Le et al., 2018). Dystrophin is a long filamentous 427 kDa protein made up of four main domains separated by hinges. In muscle cells, the continuity between the internal filamentous actin cytoskeleton and the extracellular matrix is ensured by binding of dystrophin at its N-terminus to actin filaments through an actin-binding domain (ABD1) and at its C-terminus, to β-dystroglycan. The latter protein

* Corresponding author at: Institut de Génétique et Développement de Rennes, Faculté de Pharmacie, 2 avenue du Pr Léon Bernard, 35043 Rennes Cedex, France.
E-mail address: olivier.delalande@univ-rennes1.fr (O. Delalande).
[1] Contributed equally to this work.
[2] Present address: Université de Lorraine, LIBio, F-54000 Nancy, France.

https://doi.org/10.1016/j.jsb.2019.107411
Received 3 June 2019; Received in revised form 7 October 2019; Accepted 29 October 2019
Available online 02 November 2019

spans the membrane and anchors the dystrophin glycoprotein complex (DGC) with proteins of the extracellular matrix (Ervasti and Campbell, 1991; Ibraghimov-Beskrovnaya et al., 1992). While essential regions of the dystrophin protein are located at both ends of the protein, the central domain is also thought to play a key role in regulating the membrane cytoskeleton and the extracellular matrix scaffold. This central domain of dystrophin comprises 24 spectrin-like repeats of approximately 100 residues each in which some specialized regions have been shown to interact with numerous partners such as neuronal-nitric oxide synthase (nNOS) (Lai et al., 2009), F-actin (Amann et al., 1998, 1999) and lipids (DeWolf et al., 1997; Legarnier et al., 2009). The central domain was previously described as a "rod domain". However, *in silico* (Legrand et al., 2011) and *in vitro* (Delalande et al., 2018) analyses showed that the central domain can no longer be considered as a straight and passive linker between ABD1 and the C-terminus; rather, its filamentous structure is believed to have an important and dynamic role in the scaffolding of muscle cells through interactions with the cytoskeleton (Amann et al., 1998; Sarkis et al., 2013) and membrane lipids (Zhao et al., 2016).

Mutations in dystrophin are the cause of the severe muscle wasting disease, Duchenne muscular dystrophy (DMD), a life-limiting, rapidly progressive form of muscular dystrophy which is an X-linked recessive disorder affecting 1:5000 boys (Stark, 2015) in which loss of dystrophin destabilizes muscle membranes. Internal in-frame deletion mutations in the dystrophin gene (*DMD*) that preserve the amino- and carboxyl-termini of the protein but eliminate various parts of the central domain cause the milder Becker muscular dystrophy (BMD) phenotype (Nicolas et al., 2015). As observed in BMD patients, the dystrophin protein therefore can tolerate internal deletions that maintain a shortened central domain and the amino- and carboxyl-termini regions, this BMD protein resulting in a more or less severe loss of muscle function. The severity of the disease is not simply linked to the length of the protein but much more to sophisticated and yet largely unknown functional patterns of the shortened dystrophin (Nicolas et al., 2015; Wein et al., 2015). Therapeutic strategies aim to convert DMD to the mildest BMD possible by skipping or deleting out-of-frame exons and restoring the expression of truncated forms of dystrophin protein (Yokota et al., 2012). In parallel, due to the limited packaging capacity of viral vectors, transport and expression of shortened forms of dystrophin, the so-called mini- or microdystrophins, have been developed for gene therapy (Belanto et al., 2014; Barthélémy and Wein, 2018). However, the precise consequences of in-frame deletions on the stability and function of dystrophin are not to date predictable *a priori*, this is largely due to the lack of knowledge on the molecular basis of dystrophin structure and interactions. Given that current gene therapies for DMD aim to produce shortened dystrophins, it appears essential to be able to predict their properties compared with those of the native full length molecule. This however remains dependent upon exhaustive knowledge of how wild type dystrophin interacts in muscle cells. Particularly, a full understanding at the molecular level of the interaction of ABD2 with both F-actin and membrane lipids is required. Thus, it appears crucial to analyze the structure to function relationship of the full-length native dystrophin.

Binding to F-actin is ensured through two subdomains of dystrophin. The first one, located at the N-terminus, is named ABD1 and is now well described as being composed of calponin homology domains (Singh et al., 2012; Singh and Mallela, 2012; Winder et al., 1995a). It is crucial in dystrophin since mutations of ABD1 that lead to a loss of F-actin binding represent the second-most common cause of DMD (Henderson et al., 2010). On the other hand, much less is known about the second actin binding domain (ABD2) that is located in the central domain. Early work from Ervasti's group demonstrated that in the *mdx* mouse, a rodent model of muscular dystrophy that lacks dystrophin, the entire γ-actin network is poorly connected to the sarcolemma (Sonnemann et al., 2006). This suggested a role for dystrophin in maintaining the sub-sarcolemmal F-actin network in close register with the membrane thus providing mechanical stability. Later experiments demonstrated that a proteolytic product of dystrophin comprising amino acids 1416–1880, from repeats 11 to 15 (R11-15) constituting ABD2 (Lai et al., 2009; Sarkis et al., 2013) exhibited actin binding properties, which could serve to reinforce the association of actin with the membrane. These studies established a model that suggested dystrophin binds laterally along actin filaments through the synergistic effect of two distinct low affinity binding sites, which may hold important clues to its mechanical function *in vivo* (Henderson et al., 2012). In addition it was shown that the dystrophin monomer is able to bind along the length of one single actin filament (Kumar et al., 1997; Prochniewicz et al., 2009), the binding driven at least in part by electrostatic interactions (Amann et al., 1998, 1999) and with a 1:3 to 5 ratio (Rybakova et al., 2006).

Previously, we investigated the lipid binding properties of the spectrin-like repeats of the central domain and defined that repeats 1 to 19 would be able to bind membrane models *in vitro* (Vié et al., 2010, Legarnier et al., 2009). Moreover we demonstrated that subdomain R11-15 exhibits unique lipid-binding properties, namely the ability to interact with anionic as well as zwitterionic lipids, and to adapt its interaction and organization depending on lipid packing and lipid type (Sarkis et al., 2011). From these studies, we suggested that the physiological role of the central domain of dystrophin in sarcolemma scaffolding could partly occur through modulation of lipid-protein interactions. Recent *in vivo* data are in line with our *in vitro* findings and demonstrated that at least the R1-3 and R10-12 fragments are targeted to the sarcolemma (Zhao et al., 2016).

Considering the above findings, we further hypothesized that both sarcolemma and actin filaments could bind simultaneously to dystrophin through the ABD2 subdomain, explaining the biological significance of this region *in vivo*. By surface shear rheology measurements, we showed that the central domain of dystrophin is able to create a bridge between F-actin and membrane lipids, dramatically modifying the membrane resistance to shear stress (Sarkis et al., 2013). We concluded that ABD2 creates a mechanical link which likely contributes *in vivo* to the protection of the sarcolemma from ruptures and to the shock absorber function of dystrophin in muscle cells. Molecular simulations of the dystrophin central domain (Legrand et al., 2011) suggested that R11-15 is framed by flexible junctions and therefore can be considered by itself as an independent subdomain of the dystrophin. Resolution of Small-Angle X-ray Scattering (SAXS)-based models for R11-15 (Molza et al., 2014, Delalande et al., 2018) and techniques like small-angle neutron scattering (SANS) contrast-matching (Dos Santos Morais et al., 2017), or crosslinking coupled with mass spectrometry (XL-MS) applied to the study of dystrophin-bicelle complexes (Dos Santos Morais et al., 2018) offered us new opportunities to study central domain structure and interactions at a molecular level. In the present study, we investigated by a similar approach the interactions of dystrophin ABD2 with F-actin and with membrane lipids. We conclude that both partners can together contribute to bridging cytoskeleton to sarcolemma and propose a ternary model of the complex as a step forward toward the ability to predict *a priori* the consequences of in-frame exon skipping or the properties of microdystrophins for therapeutics.

2. Material and methods

Schematic representations of dystrophin and actin are shown on Fig. S1A.

2.1. Dystrophin fragment production

All multi-repeat fragments were designed according to the alignment of Winder (Winder et al., 1995b).

Name	Recombinant protein sequence	MW (kDa)	Number of residues	ε ($M^{-1}.cm^{-1}$)
R1-3	*GS* EVNLD…QISQA	38.5	333	59,720
R11-15	*GS* FQKPA…LNFAQ	60.0	515	45,950
R8-15	(HIS_6tev*)* RKEAL…LNFAQ	100.2	861	92,360
R11-19	(HIS_6tevthb) FQKPA… LLQEL	116.8	997	113,245
ABD1	*GS* LWWEE…IQEVE	29.1	253	51,575

Residues in italics are residual residues from a thrombin cleavage site. Human dystrophin (Uniprot P11532).

2.2. DYS R1-3 cloning and expression in E. coli

The R1-3 fragment was produced and purified as previously described (Dos Santos Morais et al., 2018).

2.3. DYS R11-15 cloning and expression in E. coli

The DYS R11-15 (F_{1461}-Q_{1973}) fragment was amplified by PCR from pTG11025 plasmid DNA with the Dp427m human ORF (a gift from Transgene SA, Strasbourg France) with primers designed including an NdeI or XhoI restriction cassette (Integrated DNA Technologies) and also including a 6xHis tag sequence followed by a thrombin recognition site in the N-terminal region. PCR products were amplified with Q5 HiFi DNA polymerase (NEB), digested, purified (Macherey-Nagel NucleoSpin kit) and inserted into pET21 vector (Novagen) at the NdeI/XhoI restriction sites. The His-tagged recombinant protein was produced in *E. coli* BL21(DE3) strain after 1 mM IPTG induction for 4 h at 37 °C and purified by immobilized metal affinity chromatography (IMAC) on Ni-Sepharose column (HisTrap, GE Healthcare) according to the manufacturer instructions. The His-tag was removed by thrombin cleavage and the proteins were further purified with a size-exclusion chromatography column (HiLoad 16/600 Superdex 200 prep. grade, GE Healthcare) equilibrated with TNE buffer (20 mM Tris, 150 mM NaCl, and 0.1 mM EDTA, pH 7.5). The purity was assessed by SDS-PAGE stained with Coomassie blue. The concentration was determined spectrophotometrically using calculated molar extinction coefficients at 280 nm of 45,950 $M^{-1}.cm^{-1}$.

2.4. DYS R8-15 and DYS R11-19 cloning and expression in insect cells

Extended (8 extra aa) R8-15 (R_{1148}_Q_{1973}) and R11-19 (F_{1461}-L_{2420}) fragments were amplified by PCR as described above. The R8-15 fragment was inserted at the NcoI and XhoI sites with T4 DNA ligase (NEB) into pFastBacHT vector (Invitrogen™). The R11-19 fragment was inserted at the BamHI and XhoI sites of a previously modified pFastBacHT including a thrombin recognition site in NcoI/BamHI. The constructs were verified by sequencing (Big Dye Terminator V3, Applera) and transferred into DH10BAC cells (Invitrogen™) for recombination and bacmid DNA production. Sf9 insect cells were transfected with 1 μg bacmid DNA and Cellfectin-II reagent according to BAC-to-BAC instruction manual (Invitrogen™). Resulting baculoviruses were amplified for up to 3 passages.

Recombinant proteins were produced in Sf9 cells infected with baculovirus for 3 days at 27 °C. Cells were lysed for one hour at room temperature in phosphate buffered saline (sodium phosphate 25 mM pH8, NaCl 300 mM) containing protease and phosphatase inhibitors (Pierce), 50 μl/ml insect PopCulture® reagent (Novagen), 10 U/ml benzonase® (Novagen) and 5 mM imidazole. Lysates were clarified by centrifugation at 15,000*g*, 30 min, 4 °C; loaded onto a HisTrap excel™ Ni-NTA column (GE Healthcare, ÄKTA start instrument), washed with PBS pH8 + 5 mM imidazole. Purified proteins were eluted in phosphate buffer saline pH8 containing 50 mM imidazole then subjected to gel filtration onto a HiPrep 26/60 Sephacryl S-200HR column (GE Healthcare, ÄKTA FPLC instrument).

2.5. Actin binding domain 1 (ABD1) cloning and expression

The ABD1 fragment was amplified by PCR as described above, digested by BglII/XhoI and cloned into the BamHI/XhoI restriction sites of pGEX-4 T-1 vector (GE Healthcare). The protein was expressed in E. coli strain ER2566 (NEB) and induced at an OD 600 nm of 0.5 with 1 mM IPTG for 4 h at 37 °C. The purification was performed according to the manufacturer's instructions on a 5 mL GSTrap FF affinity column (GE Healthcare) with an Äkta start instrument and the protein was eluted by an overnight cleavage at 4 °C with thrombin at 10 unit.mL^{-1} in 20 mM Tris-HCl pH7.4, 150 mM NaCl buffer.

2.6. Bicelle preparation

Bicelles were prepared as described previously (Dos Santos Morais et al., 2017). The 1,2-dimyristoyl-*sn*-glycero-3-phosphocholine (DMPC), 1,2-dimyristoyl-*sn*-glycero-3-phospho-L-serine (DMPS), 1,2-dihexanoyl-*sn*-glycero-3-phosphocholine (DHPC), 1,2-dimyristoyl-d54-*sn*-glycero-3-phosphocholine-1,1,2,2-d4-N,N,N-trimethyl-d9 (DMPC-d67), 1,2-dimyristoyl-d54-*sn*-glycero-3-[phospho-L-serine] (DMPS-d54), and 1,2-dihexanoyl-d22-*sn*-glycero-3-phosphocholine-1,1,2,2-d4-N,N,N-trimethyl-d9 (DHPC-d35), conditioned in chloroform or chloroform/methanol, were all purchased from Avanti Polar Lipids and used without any further purification. D_2O, Tris-d11, and EDTA-d16 were from Eurisotop. Chloroform or chloroform/methanol solutions containing the appropriate amounts of either zwitterionic (DMPC/DHPC, 1:1) or anionic (DMPC/DMPS/DHPC, 0.67:0:33:1) lipid mixtures were dried overnight under vacuum. The lipids were then rehydrated in TNE or d-TNE buffer solution (20 mM Tris-d11, 150 mM NaCl, and 0.1 mM EDTA-d16, pD 7.5) to reach a total lipid concentration of at least 200 mM. The solution was then frozen in liquid N_2, thawed 10 min at 40 °C, vigorously shaken for 1 min, and centrifuged (1.5 min, 6000 rpm, MiniSpin, Eppendorf). This procedure was repeated twice, to obtain a clear suspension of zwitterionic or anionic bicelles in hydrogenated or deuterated version, denoted HZB/DZB and HAB/DAB, respectively. Stock solutions were diluted in TNE or d-TNE depending on the experiments.

2.7. Intrinsic tryptophan (Trp) fluorescence

Fluorescence measurements (two replicates) were carried out on a Fluorolog spectrofluorometer (Jobin-Yvon). Tryptophan fluorescence emission spectra were recorded in low volume quartz Hellma cells (120 μl) between 310 and 420 nm, using an excitation wavelength of 295 nm (bandwidth of 2 nm). Blanks corresponding to the buffer or bicelles alone were subtracted from the respective spectra. The protein concentration was 20 μM and the total lipid concentration was 50 mM (~150 μM of bicellar objects). The measurement temperature was 26 °C.

2.8. Circular dichroism

Quality control of all the purified proteins was assessed by circular dichroism with a JASCO J-815 (Nantes, France) spectropolarimeter with protein concentration of about 1 μM. Spectra were acquired in the range 200 – 250 nm at 20 °C with a path length of 0.2 cm. The percentage of α-helix was obtained using a 100% α-helix value of −36,000 deg.cm^2.$dmol^{-1}$ at 222 nm and the ratio of the ellipticity at 222 over 208 nm was used as an indicator of the presence of a coiled-coil as previously described (Legarnier et al., 2009). For R11-15-bicelle interactions, two replicate spectra were recorded from 200 to 240 nm in 0.02-cm pathlength Hellma cells at 26 °C. Blanks corresponding to the buffer or bicelles alone were subtracted from the respective spectra. The protein concentration was 20 μM, and the total lipid concentration was 50 mM (~150 μM of bicellar objects).

2.9. Microscale thermophoresis (MST)

Bicelles were labeled with 1 μM of 1,2-dioleoyl-*sn*-glycero-3-phospho-L-serine-N-(7-nitro-2–1,3-benzoxadiazol-4-yl) for a final concentration of 15 mM of lipids (~50 μM of bicellar objects) at $q_{eff} = 1.3$ and the [DMPC]/[DMPS] (mol/mol) ratio into the bilayer part was maintained equal to 2 (see Dos Santos Morais et al., 2018 for further information). The bicelles were titrated with a 0.75-fold serial dilution of R11-15 from 184 to 165 to 2.5–2.2 μM. The 16 solutions were then loaded into Monolith NT premium capillaries (NanoTemper) and thermophoresis was measured with a Monolith NT.115 instrument (NanoTemper). Instrument parameters were as follows: 20–30% LED power, 40–60% MST power, and 5/20/5 laser off/on/off. The measurement temperature was 22 °C or 26 °C (two technical replicates). Data were analyzed with the NT MO Affinity Analysis software v2.2.4 (NanoTemper).

2.10. Actin polymerization and sedimentation assays

Globular actin (G-actin) was prepared from rabbit muscle, as described previously (Winder et al., 1995b). Cosedimentation assays were performed as described in (Sarkis et al., 2013). Briefly, monomeric G-actin stored in G buffer (2 mM Tris, pH 8.0, 0.2 mM ATP, 0.5 mM dithiothreitol, 0.2 mM $CaCl_2$ and 1 mM NaN_3) was diluted in polymerization buffer (F buffer; final composition: 20 mM HEPES, pH 7.5, 150 mM NaCl, 2 mM ATP, 50 mM KCl, 2 mM $MgCl_2$, and 1 mM dithiothreitol) and allowed the polymerization at room temperature for 1 h. Actin polymerization was assessed by light scattering at 400 nm. For sedimentation assays, 50–100-μl samples were prepared in F-buffer in ultracentrifuge tubes. The final concentrations of actin were 5 μM and 0–150 μM for DYS R11-15. Following a 30 min incubation, samples were centrifuged for 30 min at 100,000*g* at 20 °C. Supernatants and pellets were analyzed by SDS-PAGE. Gels were stained with Coomassie blue and the amounts of proteins quantified by ImageJ software.

2.11. Click-chemistry, chemical cross-links and liquid chromatography coupled with mass spectrometry (XL-LC-MS/MS)

2.11.1. R11-15 – F-actin

F-actin and R11-15 at 5 μM final concentrations were incubated in polymerisation buffer (without DTT) for 30 min at 20 °C and then EDC ((1-ethyl-3-(3-dimethylaminopropyl)carbodiimide hydrochloride, Thermofisher scientific) was added at a concentration of 5 mM for 60 min at 20 °C. Cross-linked proteins were analyzed by SDS-PAGE stained by Coomassie blue and the bands corresponding to one actin monomer-one R11-15 monomer complexes were excised and cut into small pieces.

2.11.2. R11-15 – bicelles

HZB and HAB were labeled with 5% (mol/mol) of 1-palmitoyl-2- (9-(3-pent-4-ynyl-3-H-diazirin-3-yl)-nonanoyl)-*sn*-glycero-3-phosphocholine (pacFA PC) (Avanti Polar Lipids) bearing both photoactivable diazirine and clickable alkyne groups on one tail of the phospholipid (Haberkant and Holthuis, 2014). The modified bicelles were mixed with R11-15 to reach a final concentration of 50 mM of lipids and 15 μM of protein. Then, the protein/lipid complexes were exposed to UVA radiation (5 × 15 W, Stratalinker, GE Healthcare) for 5 min, just before SDS-PAGE analysis. The staining was performed using Coomassie blue (InstantBlue, Expedeon). The smeared parts of the gel, just above the band corresponding to R11-15, were cut into small pieces.

2.11.3. Mass spectrometry sample preparation

For both lipid-R11-15 and actin-R11-15 complexes proteins contained in the gel pieces were reduced, alkylated, and then digested with trypsin (Promega). The resulting peptides were extracted as previously described (Lavigne et al., 2012). The peptide extract was loaded (10 μl) on a nano-HPLC system (LC Packings Ultimate 3000, Dionex) equipped with a trapping precolumn (5 mm × 300 μm id, 300 Å pore size, Pepmap C18, 5 μm, ThermoScientific) and an analytical column (15 cm × 75 μm id, 300 Å pore size, Pepmap C18, 5 μm, ThermoScientific). Reversed-phase separation was performed with the same gradient as described previously (Lavigne et al., 2012). Peptides were directly eluted from the nano-HPLC column to the nanoelectrospray ion source of a LTQ-Orbitrap XL (ThermoScientific) mass spectrometer operating in data-dependent mode by automatically switching between full MS scan and MS/MS acquisitions on the 15 most intense precursor ions as described previously (Jumeau et al., 2015). MS data were saved in the RAW file format with Xcalibur 2.0.7. For the lipid-R11-15 complex, the RAW file was subjected to a database search for protein identification using Mascot Distiller 2.6.1.0 and Mascot Server 2.5.1 with its automatic decoy database search. The database searched contained the *E. coli* reference proteome from Uniprot (UP000000625, April 2017), the contaminants database from Mascot and the sequence of the R11-15 protein fragment (785 sequences, 14595443 residues). Mass tolerance was set to 10 ppm for precursors and to 0.5 Da for fragments. Trypsin was selected as enzyme with two missed cleavages allowed. Protein modifications were: fixed carbamidomethylation of cysteines and variable oxidation of methionine, and variable pacFA PC. The pacFA PC modification ($C_{39}H_{72}NO_8P$, 713.4996 Da) was manually defined in the Mascot configuration editor with a neutral loss of phosphocholine ($C_5H_{14}NO_4P$, 183.066 Da). Since the photoactivation of diazirine forms carbene intermediates that can react with any amino acid side chain or peptide backbone, all amino acids were selected as possible modified sites. Proline Studio 1.4 was used for identification validation (peptide rank = 1, false discovery rate < 1% at the peptide spectrum match level) (Carapito et al., 2015). For the actin-R11-15 complex, the RAW file was converted in the Mascot generic file format using Mascot Distiller and imported in the StavroX 3.6.6.5 (PMID: 22038510) software used to identify EDC cross-linked peptides. Cystein carbamidomethylation was selected as static modification whereas methionine oxidation was selected as variable modification. Precursor and fragment tolerances were respectively set to 5 ppm and 0.5 Da. K and R (both blocked by P) were defined as protease sites. Reported results corresponded to a false discovery rate lower than 5% (Tables S1 and S2).

2.12. Small-angle scattering (SAS)

2.12.1. Small-angle X-ray scattering (SAXS) experiments

SAXS experiments were performed as described previously (Delalande et al., 2018). Measurements were conducted at the French synchrotron SOLEIL (Saint. Aubin, France) on the SWING beamline. All experiments were performed at 15 °C. The scattering vector is defined as $q = 4\pi/\lambda \sin\theta$, where 2θ is the scattering angle. Data were collected in a q-range of 0.006–0.6 $Å^{-1}$. Data were recorded using an AVIEX170170 CCD detector at the distance of 1.8 m (λ = 1.033 Å). For the constructs R8-15 and R11-19, a stock solution of each fragment was prepared at a final concentration between 4 and 4.5 mg/ml. A volume of 60–70 μl of protein sample was injected into a size exclusion column (Bio SEC-5 500 Å, Agilent) and eluted directly into the SAXS flow-through capillary cell at a flow rate of 0.2 or 0.3 mL/min. The elution buffer consisted of NaPi 10 mM pH 7.5, NaCl 500 mM EDTA 1 mM, glycerol 2% or NaPi 20 mM pH 7.5, NaCl 300 mM, EDTA 1 mM, glycerol 2%. Two hundred fifty SAXS frames were collected continuously during the elution at a frame duration of 1.5 s and a dead time between frames of 0.5 s. One hundred frames accounting for buffer scattering were collected before the void volume. The averaged buffer scattering was then subtracted from the protein signal. SAXS curves displaying a constant Rg in a Rg versus frame number plot were averaged and were used for further characterization. Data reduction to absolute unit, frame averaging, and subtraction were performed with FOXTROT. Data were deposited in the SASBDB (Valentini et al., 2015).

R8-15: https://www.sasbdb.org/data/SASDFW4/qlng5k8cq5/
R11-19: https://www.sasbdb.org/data/SASDFX4/eqrth3wghp/

2.12.2. SAXS data analysis

Analyses were performed as described in Delalande et al. (2018). Briefly, all data processing and analysis were conducted with the Scatter software (http://www.bioisis.net/), and other programs of the ATSAS suite (Franke et al., 2017). The distance distribution function P (r) and the maximum particle diameter (DMAX) were calculated using the GNOM program. The overall ab initio models of the protein fragment R11-15 were obtained from the SAXS experimental data presented in Delalande *et al.* Ab initio models for other fragments (R8-15 and R11-19) where obtained using the GASBOR program, using 50 harmonics, the scattering profiles were fitted to a $q_{max} = 0.25$ Å^{-1} for all samples. Following a similar protocol to the one described previously, one hundred independent GASBOR computations were performed for each scattering profile, to factor the decrease in envelope convergence associated with the increased fragment size. For each fragment, the three best GASBOR computations, with the smallest χ^2, were conserved and converted to volume grid constraints (molecular shape) to guide the interactive flexible fitting simulations, as described in previous work (Molza et al., 2014). Before simulation, the homology model and the molecular shape were aligned along their longest axis. The model was then rotated 10 times around the long axis by 36° steps, followed by a 180° head-to-tail rotation to exchange N- and C-terminal end, before performing 10 more rotations. The 60 models (3 envelopes, 10 rotations, 2 directions) were adjusted afterwards. All final models were refined by standard energy minimization (Molza et al., 2014). The best models were selected upon evaluation of the final structural models obtained using PROCHECK (Laskowski et al., 1993) and DSSP (Kabsch and Sander, 1983; Touw et al., 2015) and by validation after calculating their theoretical SAXS curves with the CRYSOL program (Franke et al., 2017).

2.12.3. Small-angle neutron scattering (SANS) experiments

Preparatory work was carried out on KWS-1, KWS-2 (MLZ, Garching), and PACE (LLB, Saclay), instruments, while final investigations were done on D22 (ILL, Grenoble) instrument. Two to three sample-to-detector distances were used with a wavelength varying from 4.7 to 7 Å ($\Delta\lambda/\lambda \sim 10\%$), to cover a *Q*-range from 0.008 to 0.5 Å^{-1} for the largest one, where $Q = \frac{4\pi sin\theta}{\lambda}$ is the momentum transfer, λ is the wavelength, and 2θ is the scattering angle. All measurements were performed in 1 mm thickness Hellma *QS* cells, and the intensities obtained are in absolute units (cm^{-1}). Samples were analyzed in d-TNE buffer at 22 °C. Exactly the same buffer that had been used for bicelle rehydration was used to prepare protein/bicelle samples to guarantee a perfect buffer subtraction. Buffer exchange for R11-15 was performed by three successive diafiltrations with Amicon Ultra-15 (Millipore, MWCO 10 kDa), followed by a step with a desalting column (NAP5, GE Healthcare). The protein concentration was 93 µM (5.6 g/l) and the lipid concentration was 50 mM. Data were deposited in the SASBDB Valentini et al., 2015).

R11-15: https://www.sasbdb.org/data/SASDFT4/o4g9so8m49/
R11-15/DZB: https://www.sasbdb.org/data/SASDFU4/jvg81e6o1r/
R11-15/DAB: https://www.sasbdb.org/data/SASDFV4/rr58u3fhpg/

2.12.4. SANS data analysis

SANS data were analyzed similarly to SAXS data with the ATSAS suite and Scatter software, following guidelines unless otherwise indicated. Twenty *ab initio* models were generated with DAMMIF software (https://www.embl-hamburg.de/biosaxs/atsas-online/) by considering the data up to $Q = 0.25$ Å^{-1}. The models obtained were aligned and averaged with DAMAVER software. The presented *ab initio* models correspond to the DAMMIF model with the smallest normalized spatial discrepancy (NSD) surrounded by the corresponding DAMAVER model.

2.13. Molecular simulation

2.13.1. Low-resolution docking

Rigid low-resolution docking was performed using Ptools software (Schneider et al., 2012) to allow a large exploration of the association modes of the dystrophin ABD2 with F-actin. Given the large size of the 12-mer F-actin model (3G37, Murakami et al., 2010) we deemed it necessary to disallow edge effects upon docking the best 13 ABD2 models obtained previously from SAXS-driven flexible fitting and selected from energetic and structural criteria to allow a conformational modulation of the ligand. The ABD2 models were reduced according to the Zacharias force field (Schneider et al., 2012). The dystrophin starting position was defined using a density grid of 10 Å around the four central G-actin monomers, corresponding to 80 starting positions distributed as an open cylinder around the central F-actin part. For each model, 20,640 theoretical complexes were finally calculated, corresponding to 258 rotations applied to each starting position of the ligand (ABD2) towards the receptor (F-actin). The rigid docking results were analyzed through an energy evaluation of the theoretical complexes and by clustering procedure using a root mean square deviation of 10 Å according to the ligand final position. The best theoretical complexes are defined as the most populated clusters with the lowest ATTRACT energy for the complex. The contact frequencies between the two proteins were calculated over the 100 best clusters computed and with a cut-off distance of 5 Å between two coarse-grain particles. Peptides identified by MS analysis of the cross-linked complexes were then used to filter theoretical complexes within the same distance constraints. Interactive semi-flexible docking was performed by using BioSpring software and following the protocol described previously (Molza et al., 2014). Briefly, due to the identification of two distant interaction domains, interactive docking was performed by fixing the actin filament and either R11 or R15 in contact to the actin and by interactively bringing back the other end, unfixed, toward the filament, into a position identical to the ones identified by Ptools docking. All starting models for this interactive simulation were built through the substitution of the best positions obtained for either R11 or R15 contacts with F-actin by the ABD2 model deposited in the SASBDB.

2.13.2. Coarse-grained molecular dynamics (CG-MD) simulations

CG-MD simulations were run using the GROMACS 5.0 program with the Martini coarse-grained force field. Two protein/lipid systems were simulated in a similar way to what was done previously for the R1-3 dystrophin fragment with either zwitterionic bicelles or anionic bicelles (Dos Santos Morais et al., 2018). The R11-15 (ABD2) SAXS-based model used for the CG-MD is accessible through the online database SASBDB at http://www.sasbdb.org/data/SASDB63/ (Delalande et al., 2018). All CG-MDs were performed at a constant temperature of 303 K and under NPT conditions for the production of final CG-MD trajectories of 20 µs. Analysis was achieved with the GROMACS 5.0 tools.

3. Results

3.1. Experimental data

3.1.1. Dystrophin ABD2 binds F-actin via repeats R11 and R15

Binding assays show that in our experimental conditions ABD2 binds F-actin with a Kd of ~9 µM with a Hill coefficient of ~ 1.9 (Fig. S1B). Following incubation of F-actin with ABD2, the zero-distance cross-linker EDC was added and the products were first analyzed by SDS-PAGE (Fig. 1). R1-3 and ABD1 (actin binding domain 1) fragments of dystrophin were used as negative and positive controls respectively.

A specific EDC induced band corresponding to the expected size of one actin linked to one R11-15 is observed with an apparent MW of ~100 kDa (Fig. 1A, red arrow). No non-specific signal was observed in the absence of EDC. When F-actin alone was incubated with EDC, a 130–140 kDa band was identified as an actin multimer (blue arrow in Fig. 1A and B and Fig.

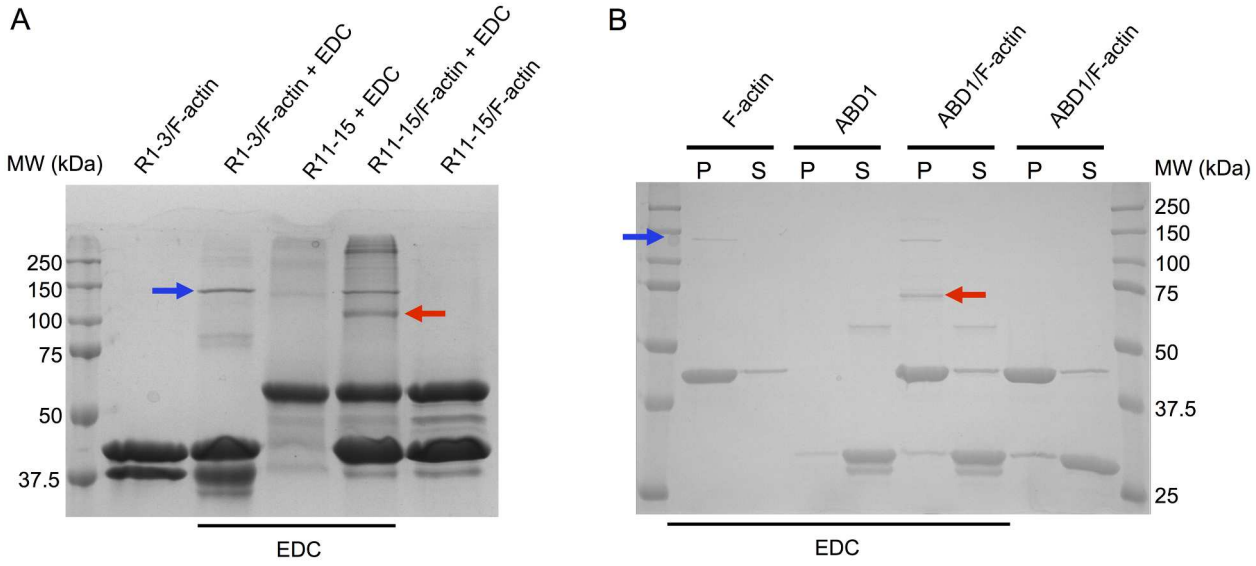

Fig. 1. (A) SDS-PAGE analysis of EDC induced F-actin-dystrophin central domain adducts. F-actin and R1-3 as a negative control, or R11-15 dystrophin fragments at final concentrations of 5 µM were incubated in the presence or absence of 5 mM of the EDC cross-linker for 1 h at 20 °C. Bands of interest were excised, trypsin digested and analysed by MS. Blue arrow: 130–140 kDa band corresponding to EDC crosslinked multimer of actin. Red arrow: band corresponding to the expected size of one monomer of R11-15 (ABD2) EDC-covalently cross-linked to one monomer of actin. (B) SDS-PAGE analysis of EDC induced F-actin-dystrophin ABD1 (actin binding domain 1) displayed as a positive control. 5 µM of F-actin and ABD1 domain alone or together were incubated in the presence or absence of EDC. Samples were centrifugated at 100.000 g. Pellets (P) and supernatants (S) were loaded on SDS-PAGE gels. Bound proteins sediment with F-actin in pellet. Bands of interest were excised, trypsin digested and analysed by MS. Blue arrow: the Actin multimer as found in (A). Red-arrow: the specific band corresponding to a monomer of ABD1 EDC-covalently cross-linked to a monomer of actin.

S1C). In the R1-3F-actin EDC mixture Fig. 1A lane 3), the actin polymer is present at 130–140 kDa, a band at ~85 kDA was identified as a R1-3 multimer and no cross-linked peptides from either proteins were identified. ABD1 used as a positive control is found specifically cross-linked to actin in a ~70 kDa heterodimer (Fig. 1B red arrow). MS results are shown in Tables S1 and Appendix Tables S1.

From the 100 kDa EDC induced band (Fig. 1A, red arrow), among the trypsin proteolysis products identified by MS, the peptides derived from actin that are found cross-linked with peptides derived from ABD2 are shown in Table S1 and Fig. S1C. The two peptides from actin isolated by MS with a high confidence are delimited by Ala21 and Arg30 or Val98 and Lys115. This means that the region of actin which is in close contact with dystrophin ABD2 resides principally in subdomain 1 (Fig. S1A). Corresponding results defining the contact mapping on the dystrophin ABD2 fragment characterize several peptides involved in the interaction with F-actin. Interestingly all are included in repeats R11, R12 or R15. These fragments are delimited by Phe1461 to Arg1470, Ser1517 to Arg1527, Lys1533 to Lys1539 and Leu1550 to Lys1568 in repeat R11, by Lys1645 to Lys1652 in repeat R12 and Lys1922 to Arg1930 in repeat R15.

3.1.2. Lipid interaction with dystrophin slightly alters its structural organization but does not overlap with F-actin contact regions

We characterized the ABD2-lipid interactions using bicelles as a membrane mimic, in a similar approach to what we have done previously for R1-3 (Dos Santos Morais et al., 2018). First, the protein/bicelle interactions were highlighted using Trp intrinsic fluorescence measurements, in the presence of either zwitterionic (HZB) or anionic (HAB) bicelles. A small increase in fluorescence was observed (Fig. S2A) and confirmed the interaction. We then used circular dichroism (CD) to probe potential structure modifications of dystrophin ABD2 during its interaction with both types of bicelles (Fig. S2B). Our first observation is that the CD spectra of ABD2 alone is typical of a predominantly α-helical structure with the presence of two minima at 222 and 208 nm, suggesting that the recombinant protein is properly folded. Moreover, the $\theta_{222}/\theta_{208}$ ratio is close to or above unity, which is evidence of an overall coiled-coil tertiary structure (Vié et al., 2010). The CD spectra of R11-15 alone or in the presence of both types of bicelles are very similar suggesting that the secondary and tertiary structures of ABD2 are maintained during binding to bicelles. Finally, we used microscale thermophoresis (MST) to determine the dissociation constant (Kd) of the complexes. A Kd value of ~10 µM was determined for the system formed by ABD2 with both types of bicelles (Fig. S2C and D).

To investigate the potential 3D structural modifications of ABD2 upon lipid binding, we performed SANS experiments on ABD2 in the presence of either zwitterionic (DZB) or anionic (DAB) contrast-matched deuterated bicelles (Dos Santos Morais et al., 2017) (Fig. 2A).

SANS measurements show that no change is observed in the case of dystrophin ABD2 interaction with zwitterionic bicelles whereas the interaction of dystrophin ABD2 does alter the fragment tertiary structure upon binding to anionic bicelles (increase of ~60 to ~80 Å of Rg towards free fragment, confirmed by the increase of D_{max} on P(r) plot in Fig. 2A inset. The best *ab initio* models computed from the SANS experiments for the dystrophin fragment in the presence of bicelles are shown and demonstrate a very high degree of similarity of the protein shape in solution by comparison to the models obtained from SAXS experiments (Fig. S3). Finally, an accurate mapping of the interaction between R11-15 fragment and both types of bicelles was investigated by XL-MS. The protein–bicelle-pacFA complexes were submitted to UV cross-link and analyzed by SDS-PAGE (Fig. 2B). If one or two pacFA fatty acids covalently cross-linked to ABD2, the increase in apparent MW would be only slight. Therefore, the smeared upper parts of the bands corresponding to ABD2 with putatively associated lipid(s) were cut from the gel and their trypsinolysis products were analyzed by MS. No peptide-lipid cross-link was identified in samples corresponding to the zwitterionic bicelle protein complex. Interestingly however, one peptide from ABD2 was identified linked to the pacFA fatty acid in the sample derived from the anionic bicelles. The score obtained for the dystrophin ABD2 peptide bearing a pacFA modification is presented in Table S2 (see also Appendix for details), this peptide ($_{1667}$AEE…YQK$_{1679}$) belongs to the C-terminal end of helix C in repeat R12 of the dystrophin domain.

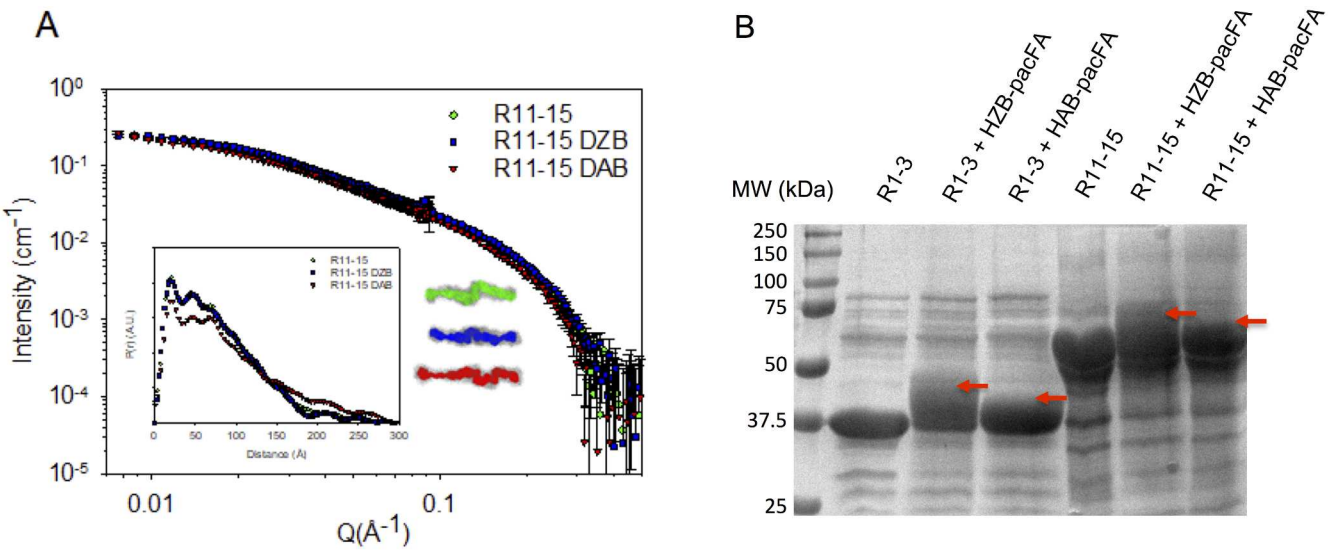

Fig. 2. (A) SANS scattering curves of dystrophin R11-15 fragment either free (green) or in interaction with zwitterionic bicelles (DZB) (blue) or anionic bicelles (DAB) (red). Inset: (left) Pair-distribution function P(r) analysis with the same color code showing a slight increase of Dmax of R11–15 when the protein fragment is in interaction with anionic bicelles and (right) ab initio models corresponding to the DAMMIF associated models (colored) with the smallest normalized spatial discrepancy (NSD) are shown, surrounded by their relative DAMAVER models (grey). (B) SDS-PAGE analysis of R1-3 and R11-15, alone or following incubation with zwitterionic-pacFA or anionic-pacFA bicelles and light-induced cross-links. The upper part of the band containing putative protein-lipid covalent complexes were cut into small pieces and analyzed by MS (red arrows).

3.1.3. Dystrophin ABD2 interacts in vitro with both F-actin and membrane lipids simultaneously

Ternary complexes comprising F-actin–dystrophin ABD2–bicelles were studied *in vitro*. Only anionic bicelles were selected for these experiments, due to the nature of the lipids found at the inner face of the sarcolemma (Fiehn et al., 1971) and to our previous observations (Legarnier et al., 2009; Sarkis et al., 2011). The EDC-cross-linked ABD2/F-actin complex was first achieved as described above, then anionic bicelles containing the pacFA lipid were added and light-induced cross-linking was performed. The result of SDS-PAGE analysis of the samples is shown on Fig. 3A.

Four bands including R11-15 smear, CL1 (~100 kDa), CL2 (~130 kDa) and CL3 (~170 kDa) were analysed by MS. Results are shown in Table S1 (complete version in Appendix). Actin and R11-15 cross-peptides were found in the CL1, CL2 and CL3 bands but not in the smear band. Interestingly, the 100 kDa band, as observed from the experiment presented in Fig. 1, was identified as a cross-linked complex between actin and R11-15. In this complex, the peptide from R11-15 ($_{1667}$AEEWLNLLLEYQK$_{1679}$) is found linked to the pacFA. All findings are summarized in Fig. 3B. In the R11-15 (ABD2) model, the peptides associated with actin peptides are highlighted in orange. All are located exclusively in repeats R11, R12 and R15. The peptide from helix C in repeat 12 of ABD2 was, as earlier observed in a binary ABD2-bicelle complex, found associated with lipids (highlighted in green).

Actin binding peptides are located exclusively in repeats R11, R12 and R15 and the lipid binding peptide is located in repeat R12. More precisely, actin and lipids bind clearly on opposite extremities of helix C in repeat 12. While all the cross-link experiments were achieved with F-actin filaments, for clarity, we report on a monomer model of actin the peptides bound to ABD2 (Fig. 3C). This model shows that the areas of G-actin bound to ABD2 do not correspond to monomer–monomer interactions but to solvent accessible domains on a double-stranded actin filament. All together these results strongly suggest that dystrophin ABD2 can interact together with F-actin and membrane lipids.

3.2. Molecular modeling data

3.2.1. Dystrophin ABD2 in solution is a well-structured subdomain

We sought to propose a structural model of the dystrophin ABD2 bound to F-actin in accordance to the experimental mapping obtained here. Therefore, we first needed to improve the analysis of SAXS data previously acquired before the launch of molecular docking computations (Fig. S3A and B and see Supporting Information). Over the 60 geometries optimized under SAXS restraints, we observe that the four best new models for ABD2 converge remarkably (Fig. S3C) including major kinks between R12 and R13 and between R14 and R15. The improved method used here therefore allows us to confirm the main topographical organization emerging from the *ab initio* treatment of SAXS data, ie the location of major kinks in the ABD2 subdomain. We also noticed that the acute R14-R15 kink is remarkably well conserved with an angle close to 81 ± 6° between main axis of the two R14 and R15 coiled-coils. However, the relative position of the R11-12 tandem towards the rest of the fragment differs slightly from one model to another due to possible changes in the R12-13 linker organization. Surface properties of the ABD2 fragment illustrate the ambivalent behavior of this subdomain well, in that it is highly stable in aqueous buffer but is also able to bind lipids *in vitro* (Fig. S3D and E).

3.2.2. Electrostatics drive the preferential binding of the ABD2 model to F-actin through repeats R11 and R15

Rigid low-resolution docking simulations were achieved by using previously selected R11-15 SAXS-based models as ligand, and with F-actin structure as receptor (Fig. S4). As a first step, we computed more than 20,000 theoretical complexes per ABD2 conformer with an almost exhaustive approach and without any restraints from the contact mapping obtained experimentally. After projection of all docking contacts on a single G-actin for a cumulative analysis of the contact frequencies of dystrophin onto the F-actin (Fig. S4A), it appears that dystrophin ABD2 does interact in a preferential manner with subdomains 1 and 3 of a given G-actin unit (Fig. S4B). The highest contact frequencies that were observed for the dystrophin ADB2 interacting with F-actin essentially concern repeats R11 and R15, the two most zwitterionic repeats of ABD2 (Fig. S3E and D). These observations are in good agreement with the experimental mapping obtained from XL-MS analysis (Fig. 3B). In a second analysis step of the calculations, the contact frequencies were filtered by only keeping the theoretical complexes that were in accordance with the ABD2–F-actin mapping experiments (Fig. 4A, Fig. S4C and E).

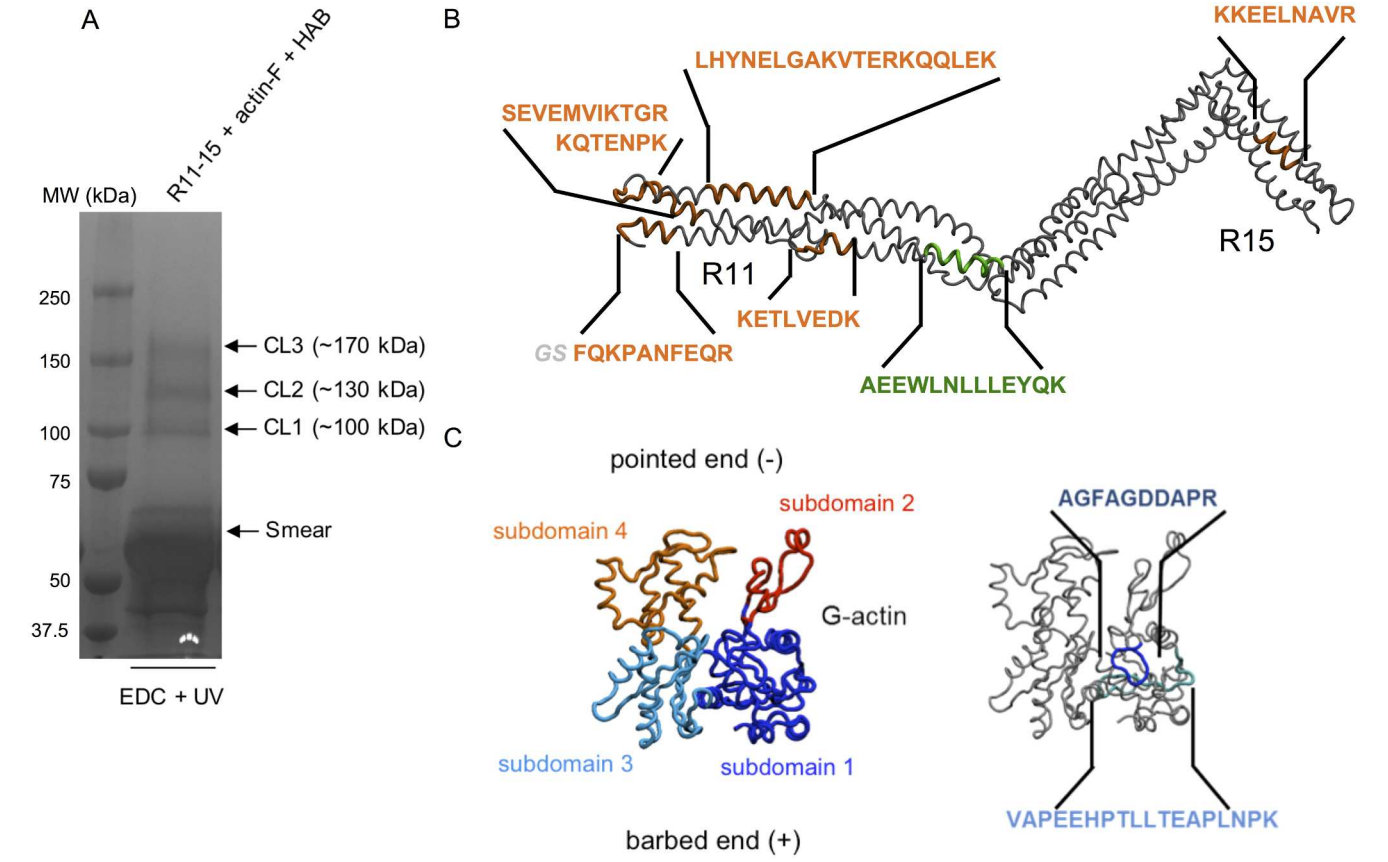

Fig. 3. (A) SDS-PAGE analysis of the F-actin-R11-15-pacFA ternary complexes. R11-15 and F-actin were submitted to EDC cross-link. Then the products were incubated in the presence of anionic bicelles containing pacFA (HAB-pacFA) before light activated cross-linking; Coomassie blue staining. CL1 Arrow: ~100 kDa band corresponding to one monomer of R11-15 cross-linked to one monomer of actin (as in Fig. 2B) and putatively associated with the pacFA lipid (additional MW of 1 kDa not detectable by SDS-PAGE). Additional CL2 and CL3 bands corresponding to cross-linked multimers. R11-15 smear, CL1, CL2 and CL3 were excised and analyzed by mass spectrometry. (B) Peptides experimentally identified to contact F-actin (orange) and anionic bicelle (green) mapped on the backbone of the dystrophin ABD2 fragment (grey); (C) 3D model of G-actin (PDB 3G37) showing the actin monomer standard subdomains; right: Peptides from actin experimentally identified to contact ABD2 (blue) mapped on the backbone of a single G-actin unit (grey).

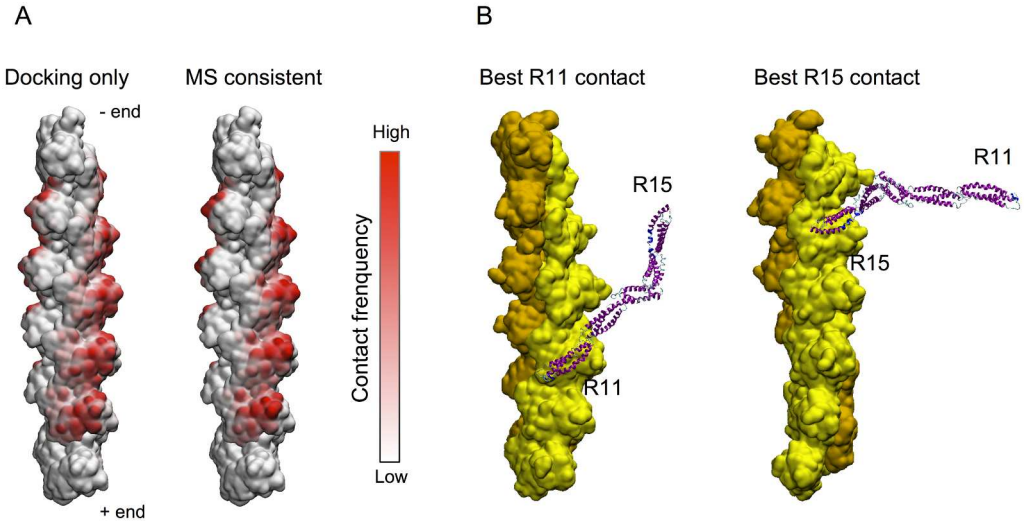

Fig. 4. (A) Contact frequencies of the dystrophin ABD2 with the F-actin structure all over the docking simulations: raw data obtained by rigid low-resolution docking (left) and same data after filtering of the sole solutions in accordance to experimental mapping (right). (B) Best (Attract energy and cluster size) theoretical complexes computed for the association of dystrophin (purple and blue) ABD2 to the F-actin (yellow and orange) show two main independent groups of solutions verify experimental mapping. The first cluster shows a great accordance concerning the experimental interaction with repeat R11 and F-actin (left), as the other one shows a great accordance concerning the experimental interaction between repeat R15 and F-actin (right).

Finally, it confirmed that ABD2 contacts F-actin at a site far from the interface defined by the contact region of subdomains 3 and 4 of different actin subunits, when associated in a filament. Following the standard analysis proposed by Attract and based on an internal energy ranking and geometrical clustering of ligand poses, the best ABD2–F-actin theoretical complexes were selected (Fig. 4B). In these models, repeat R11 of ABD2 binds preferentially in a manner that enables the orientation of the dystrophin filament in the same direction as the main axis of F-actin, forcing a small contact site at repeat R12 due to its proximity. Nevertheless, it also clearly shows the disengagement of the main part of repeat R12 from close contact with the actin filament thanks to a moderate kink at the R11-R12 linker. On the contrary,

repeat R15 contacting models highlight that the acute kink characterized at the R14-15 linker (Delalande et al., 2018) could play an essential role in accommodating the two F-actin and dystrophin filaments. It appeared at this stage that none of these models could verify a double contact from both repeats R11 and R15 in the same complex (Fig. 4B), as we can hypothetize from co-sedimentation assay analysis and Kd measurements found in the literature (Amann et al., 1998, 1999; Rybakova et al., 2002). Nevertheless, these docking simulations provided high quality orientations for each isolated R11/R12 and R15 repeats towards F-actin. They were then further used as starting structures for final improvements incorporating ABD2 flexibility.

3.2.3. The ABD2 model could contact two different strands of the F-actin microfilament

Interactive flexible docking is a technique to improve docking models as we already discussed earlier (Molza et al., 2014). Through interactive simulations, we explored the multiple possibilities in the positioning of repeats R11 and R15 relative to each other, both in terms of distance (number of actin units separating each contacting monomer from + 1 to + 6) and topology (same strand of microfilament or not). To achieve this, we fixed either the position of repeat R11 or of repeat R15 according to the best models obtained from rigid docking (principle shown in Fig. 5A).

All the best models computed by this approach derived from the same type of simulations, namely the one in which repeat R11 was restrained and the rest of the dystrophin ABD2 was driven to investigate the contacts experimentally mapped on repeat R15 (Fig. 5A and 5B). By closely characterizing the main properties of the molecular surfaces involved in the interaction between ABD2 and F-actin, we conclude that electrostatics should play a key role in the association (Fig. 5C). However, the edge of the actin filament accommodating repeat R15 of dystrophin could also be crucial for the stabilization of the complex through specific hydrophobic patches (Fig. 5D). Finally, after comparison of contact analysis of our best models with the experimental mapping, we can conclude that repeats R11 and R15 in ABD2 are ideally located on opposite strands of F-actin (Fig. S4F). Simulations bearing the best evaluation criteria (see Material and Methods) show a contact analysis with repeats R11 and R15 separated by + 5 actin subunits along the F-actin filament. Interestingly, co-sedimentation assays have a stoichiometry of 1 to 3, suggesting that a single R11-15 fragment binds twice to an actin filament every 6 actin monomers. However, the simulation results associated with a contact every 3, 4 or 6 actin subunits would lead to structural features not compatible with experimental data. For the + 3/+4 actin monomers hypothesis, this would imply a thermodynamically unfavorable bending of the dystrophin filament. For the + 4/+6 actin monomers hypothesis, this would result in continuous contact with actin all along the dystrophin fragment (Fig. S4F), which would be incompatible with MS data and with the lipid interaction map (see later). Consequently, these results suggest that the dystrophin filament should follow the F-actin helicity through a double contact with two opposite strands of the same microfilament.

3.2.4. Dystrophin binds to both anionic and zwitterionic bicelles at their outer toroidal surface

Low-resolution molecular dynamics (CG-MD) simulations have been used to explore molecular mechanisms that could lead to ABD2-bicelle interactions, and considering zwitterionic bicelles as a control. First, during CG-MD simulations, the dystrophin ABD2 is slowly recruited by zwitterionic bicelles whereas it is quickly and spontaneously bound to anionic bicelles (Fig. S5A and B). But more interestingly, we observe a very different relative position of the dystrophin ABD2 fragment towards each bicelle type (Fig. S5C and D). Both interact with the tore part of the disk, a region with an increase in packing defects and is thus more hydrophobic. ABD2 at this stage is only contacting zwitterionic bicelles through repeat R15 whereas R11 to R13 repeats lie all along the anionic bicelle side. It is noteworthy, that the peptide identified by XL-MS for the R11-15/HAB complex was found in repeat R12, in agreement with the CG model obtained. The different features observed in MD simulations can be related to the moderate conformational changes of dystrophin ABD2 observed by SANS, as the more expanded contact of ABD2 with anionic bicelles could diminish the kinks observed in solution at the linkers and therefore result in a more elongated structure.

3.2.5. Dystrophin R4-19 model is compatible with a simultaneous accommodation of the ABD2 interactions with F-actin and sarcolemmal lipids

In contrast to dystrophin ABD1 which is a subdomain separated by hinge H1 from the central domain, (see Fig. S1A) ABD2 belongs topologically to a long R4-19 fragment delimited by hinges H2 and H3. Our previous structural study of the central domain highlighted kinks at

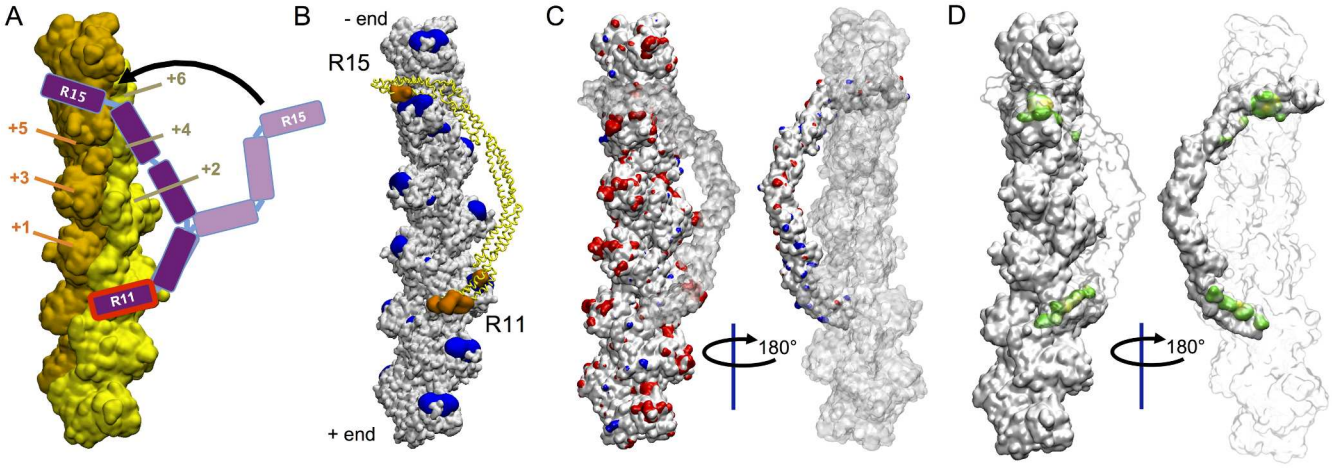

Fig. 5. (A) Principle of the flexible docking. In this example, the dystrophin repeat R11 is fixed on the actin filament following the best pose obtained by the previous docking step. During the interactive simulation, the rest of the ABD2 fragment is driven to fit the experimental contact obtained for the dystrophin repeat R15. The two R11 and R15 repeats of ABD2 contacting the F-actin could be spaced from +1 to +6 actin monomer from each others but with different effects on the structure stability of the dystrophin. (B) Structure of the best model for the complex formed by the dystrophin ABD2 (yellow cartoon) and F-actin (grey volume) and verifying both contacts of the dystrophin repeats R11 and R15 with the actin filament. Peptides identified by experimental mapping are shown as a blue volume for F-actin and as an orange volume for dystrophin. (C) and (D) electrostatic and hydrophobic molecular potentials for the characterization of the interacting surfaces between both proteins; (C) Electrostatic potential is set for isovalues of ± 50kTe (blue for positive and red for negative, from APBS calculations); (D) Molecular Hydrophobic Potential (MHP from Platinum calculations, see Pyrkov et al., 2009) with normalized values ranging from −1 (green, hydrophillic) to +1 (yellow, hydrophobic).

specific linkers. However some missing features remained for the R10 repeat – and consequently for R9-10 and R10-R11 linkers – and for the R15-16 mini-hinge. As the study of ABD2 interactions with partners could suffer from these missing structural data, we produced R8-15 and R11-19 dystrophin fragments and analyzed them by using the small-angle X-ray scattering approach combined with interactive flexible fitting techniques (Molza et al., 2014). Both fragments were expressed in insect cells, and purity was assessed by SDS-PAGE (Fig. S6A). CD spectra show that both proteins exhibit a typical mainly coiled-coil structure (Fig. S6B) and SAXS curves typical of non aggregated proteins with elongated shapes were obtained (Fig. S6C). Global parameters measured indicate that the radius of gyration were 100 Å for R8-15 and 90 Å for R11-19 (Fig. S6D). Thus the dystrophin R11-19 fragment is less elongated in solution than the R8-15 fragment, despite the presence of one additional repeat. This feature is well illustrated by the best *ab initio* models generated for each of the fragments (Fig. S6D and F). High quality $\chi 2$ values of their related theoretical SAXS curves (2.5 to 2.6 for R8-15 and 0.8 to 0.9 for R11-19) and the great convergence of their *ab initio* models (NSD < 3.4 Å for R8-15 and NSD < 3.8 Å for R11-19) support the relevance of using these models as a volume guide for flexible fitting. The SAXS-based atomic models obtained for these two new central domain fragments (SASDFW4 and SASDFX4 in the SASBDB), were finally used to produce an extended three-component complex with F-actin, dystrophin R4-19 and a membrane model. By maximizing the overlapping regions of the newly characterized fragments (R8-15 and R11-19) and the fragments previously modelled (R4-9, R11-15 and R16-19) (Delalande et al., 2018), we proposed a R4-19 subdomain model in good agreement with the kinks previously defined at the linker regions (Fig. S7A and B). Positioning of the complete R4-19 SAXS-based model according to the theoretical model of ABD2–F-actin was achieved without structural outliers (Fig. 6).

4. Discussion

4.1. Dystrophin ABD2 is defined by two interaction subdomains localized in repeat R11 and repeat R15

Until now, the boundaries of the dystrophin second actin binding domain were still under debate as authors firstly proposed an interacting region ranging from repeat R11 to repeat R17 (Rybakova et al., 1996; Amann et al., 1998), whereas later studies showed that R11-15 was sufficient for the binding of the dystrophin central domain to F-actin (Sarkis et al., 2013). Due to protein fragment expression and stability, we chose to limit the ABD2 region to R11-15 and confirmed the presence of contact patches involving a large part of repeat R11 (and a small neighbouring site in R12) and a short region within repeat R15. On the actin side, we described for the first time subdomains 1 and 3 to be the main regions interacting with the dystrophin central domain. These results seem to be coherent with the molecular surface potentials computed from structure and models of both protein partners. Indeed, F-actin is electrostatically highly negative and as predicted from our systematic potential analysis proposed earlier, so are the dystrophin repeats (Legrand et al., 2011). It is notable however, that R11 and R15 are the two most zwitterionic repeats of the R11-15 dystrophin fragment. This could facilitate an association between both filaments even through a mechanism mainly based on electrostatics as suggested earlier (Amann et al., 1998). In addition, the experimental mapping procedure naturally provides peptides from both partners linked in most of the cases by salt-bridge interactions in the native complex, as the EDC chemical cross-linker is bridging acidic and basic residues. This might artificially emphasize the importance of electrostatics in our case, given also that hydrophobic regions could play a significant role in the association of the dystrophin filament with F-actin, as they comprise the core of the binding sites. Finally, we propose that dystrophin would use repeats R11/R12 and R15 to contact two different strands of the actin filament with a distance of + 5 actin subunits between them, in accordance to a two binding site model fitted to binding assays. Measurement of average distances in the models between R11 and R15 repeats and between two actin subunits distant from + 5 (~170 Å and ~140 Å, respectively) seem to strengthen this hypothesis as other positions computed for dystrophin towards F-actin have shown to be unrealistic in terms of topological organization. It is also noticeable that stoichiometry assays we performed (1:3 for ABD2:G-actin) strongly support these results if we consider that dystrophin can fully decorate F-actin. Nevertheless, specific cross-linking of a single ABD2 simultaneously on two actin monomers could have not been observed through MS mapping, probably due to the relative rarity of EDC crosslinking event.

4.2. Dystrophin actin-binding domain 2 allows structurally non-overlapping interaction with F-actin and phospholipids

As the two main binding interfaces of ABD2 are located on the widely spaced repeats R11 and R15, it can be defined as a non-continuous subdomain of the dystrophin central domain. This is compatible with the location of the lipid binding site of ABD2. Indeed, we accurately characterized dystrophin repeat R12 as the major binding region with anionic bicellar systems. This result is also consistent with the results obtained by Zhao et al. that showed the R10-12 dystrophin fragment to be a lipid-binding domain *in vivo* (Zhao et al., 2016). In previous work, our *in vitro* studies correlated well with *in vivo* studies by the same authors, all together leading to the conclusions that the R1 repeat of dystrophin central domain exhibits membrane lipids binding properties. For the ABD2 interaction with lipids, it is noticeable that from our MD simulations, dystrophin ABD2 preferentially binds to the outer toroidal surface of the bicelle, a region exhibiting packing defects

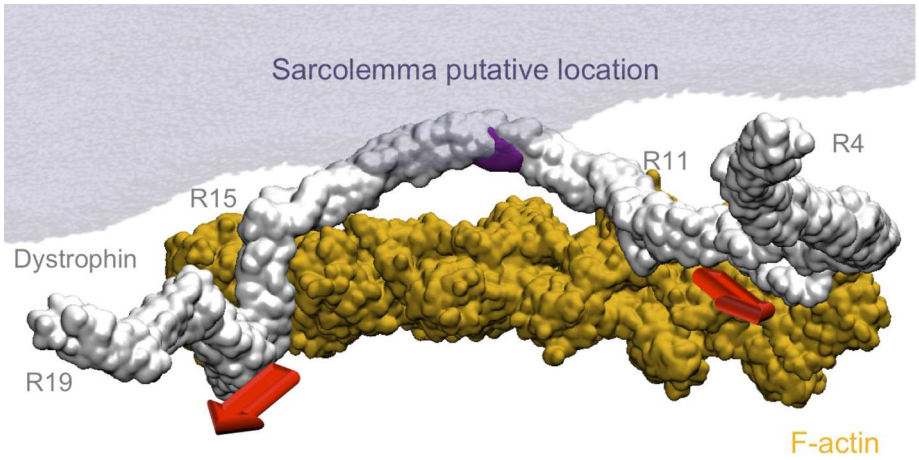

Fig. 6. Final structural model of the DYS R4-19 subdomain (white molecular surface) bound to F-actin (orange) and sarcolemma (violet) through contact peptides identified by cross-link chemistry and mass spectrometry. Repeats R11 and R15 are in contact with F-actin while R12 may be simultaneously in contact with membrane lipids (purple). Extension to N-terminal and C-terminal ends of ABD2 allow to observe the disengagement of dystrophin central domain from the F-actin binding area (red arrows), and this should result in the reduction of steric hindrance in the case of interaction with other cellular partners.

(Dos Santos Morais et al., 2018). This observation highlights that the interaction of dystrophin with phospholipids would be mainly stabilized by hydrophobic interactions. This hypothesis is also supported by experimental mapping results as the location of the clickable chemical group on the UV-photoactivable lipids is at the very end of their aliphatic chain. Indeed, the pacFA is a long-chain phospholipid that should be buried in the bilayer part of the bicelle and the end of its aliphatic chain carrying the clickable chemical group should only be accessible to a protein on the outer toroidal surface of the bicelle thanks to packing defects. However, the specific behavior of dystrophin towards anionic bicelles but not towards zwitterionic bicelles indicate that electrostatics or hydrogen bonding could also play a minor role in the recruitment or in the stabilization of dystrophin-sarcolemmal interactions.

One major conclusion from our work is that the lipid binding region does not overlap with the actin binding regions suggesting a possible simultaneous interaction with these two components. This result is consistent with our previous work based on the trypsin proteolysis assay of ABD2 bound to lipid vesicles (Sarkis et al., 2011). The integrative structural model that we propose is in keeping with the experimental restraints related to the structure of the dystrophin central domain (DYS R4-19) and the ABD2 interaction patterns with F-actin and lipids. The binding of ABD2 to F-actin as measured by co-sedimentation assays has a Kd of ~9 μM, in accordance with what was reported previously (Amann et al., 1998). Interestingly by microscale thermophoresis, we measured a similar Kd of ~10 μM for the interaction of the same ABD2 fragment with both kinds of bicelles. These observations could be of a great importance if verified in a cellular context.

4.3. Dystrophin actin-binding domain 2 as a structural relay for dystrophin-actin-lipid complex

The location of the R11-15 lipid and actin binding domain, right on the middle of the dystrophin central domain suggests it could act as a tether, keeping the dystrophin close to the membrane and to the subsarcolemmal cytoskeleton. This function would be otherwise only achieved by the widely distant ABD1 (at the N-terminal end) and beta-dystroglycan anchoring (at the C-terminal end) (Chen et al., 2003). This is supported by the fact that currently designed micro-dystrophins that restore part of the muscle resistance to mechanical stress in animal models (Ramos et al., 2019) exhibit large internal deletions in the central domain. In all cases ABD2 is missing in these therapeutic proteins. In addition, very mild forms of BMD are observed in patients lacking large parts of the central domain including ABD2 (Nicolas et al., 2015). Dystrophin ABD2, apparently dispensable in shorter proteins, could help to keep the dystrophin filament correctly localized all along length of the native protein. However, given that the central domain is believed to act as an interaction hub, a large deletion in it could lead to some loss of partners (like nNOS or syntrophin, Molza et al., 2015). One hypothesis is that, when the full length protein is present in healthy people, a spatial intermediary scaffolding function including a bridge between membrane and cytoskeleton actin would be necessary. This seems largely counteracted by the benefit of bringing the N-terminal end closer to the C-terminals end, eliminating the need for a central tether. In conclusion, the physiological role of ABD2 remains to be fully established. It appears to be dispensable in some mild BMD or in therapeutic micro and minidystrophins. An intermediary scaffolding role would be necessary for the full length protein but unnecessary when the protein is very short.

One however has to keep in mind that severe BMDs may be observed with either ABD2 being present or not, as many other structure to function features in dystrophin are involved and to date not fully understood. For all gene therapy strategies in progress (Duan, 2018) for muscular dystrophies that aim to express shortened dystrophins, fundamental knowledge of structure to function relationship of the protein is required.

5. Short conclusion section

Most gene therapy strategies for muscular dystrophies aim to express shortened dystrophins. Fundamental knowledge of structure–-function relationships of the protein is required. In this paper we show that the interaction of actin binding domain 2 in the central domain of dystrophin with filamentous actin is achieved through selected areas in spectrin-like repeats 11 and 15. On the other hand, lipids are found to interact only with repeat 12 in ABD2. The lipid binding region does not overlap with the actin binding regions. This suggests a simultaneous interaction of ABD2 with these two components. Both partners can contribute together to tether the cytoskeleton to the sarcolemma. We propose a ternary model of the complex in agreement with experimental constraints. This represents a step forward toward the ability to predict *a priori* the consequences of in-frame exon skipping or the properties of microdystrophins for therapeutics.

Author contributions

The manuscript was written through contributions of all authors. All authors have given approval to the final version of the manuscript.

Funding sources

This research was supported by research grants from the AFM–Téléthon (Application #018211A) and the french GENCI computing program (DYSIM project). DML was recipient of a PhD fellowship from AFM-Téléthon (grant 19409). RDS was a recipient of a PhD fellowship from the Conseil Régional de Bretagne (BZH ARED #8893) and the laboratoire Leon Brillouin and Synchrotron SOLEIL (thesis #2014).

.

Declaration of Competing Interest

The authors declare that they have no known competing financial interests or personal relationships that could have appeared to influence the work reported in this paper.

Acknowledgments

We thank C. Tascon (Protein purification facility, UMR-CNRS 6290), the Spectroscopies-DCTP core facility from BIOSIT at the University of Rennes. We also wanted to acknowledge Tim Pyrkov for providing stand-alone version of Platinum for the calculations of MHP on a large amount of structures. The authors are also grateful to Giulio Gambarota for his careful reading of the manuscript.

Appendix A. Supplementary data

Supplementary data to this article can be found online at https://doi.org/10.1016/j.jsb.2019.107411.

References

Amann, K.J., Renley, B.A., Ervasti, J.M., 1998. A cluster of basic repeats in the dystrophin rod domain binds F-actin through an electrostatic interaction. J. Biol. Chem. 273, 28419–28423.

Amann, K.J., Guo Athena, W.-X., Ervasti, J.M., 1999. Utrophin lacks the rod domain actin binding activity of dystrophin. J. Biol. Chem. 274, 35375–35380.

Barthélémy, F., Wein, N., 2018. Personalized gene and cell therapy for Duchenne muscular dystrophy. Neuromuscul. Disord. 28 (10), 803–824.

Belanto, J.J., Mader, T.L., Eckhoff, M.D., Strandjord, D.M., Banks, G.B., Gardner, M.K., Lowe, D.A., Ervasti, J.M., 2014. Microtubule binding distinguishes dystrophin from utrophin. Proc. Natl. Acad. Sci. U.S.A 111, 5723–5728.

Campbell, K.P., Kahl, S.D., 1989. Association of dystrophin and an integral membrane

glycoprotein. Nature 338, 259–262.
Carapito, C., Lane, L., Benama, M., Opsomer, A., Mouton-Barbosa, E., Garrigues, L., Gonzalez de Peredo, A., Burel, A., Bruley, C., Gateau, A., Bouyssié, D., Jaquinod, M., Cianferani, S., Burlet-Schiltz, O., Van Dorsselaer, A., Garin, J., Vandenbrouck, Y., 2015. Computational and mass-spectrometry-based workflow for the discovery and validation of missing human proteins: application to chromosomes 2 and 14. J. Proteome Res. 14 (9), 3621–3634.
Chen, Y.J., Spence, H.J., Cameron, J.M., Jess, T., Ilsley, J.L., Winder, S.J., 2003. Direct interaction of beta-dystroglycan with F-actin. Biochem. J. 375 (Pt 2), 329–337.
Delalande, O., Molza, A.-E., Dos Santos Morais, R., Chéron, A., Pollet, É., Raguenes-Nicol, C., Tascon, C., Giudice, E., Guilbaud, M., Nicolas, A., et al., 2018. Dystrophin's central domain forms a complex filament that becomes disorganized by in-frame deletions. J. Biol. Chem. 293 (18), 6637–6646.
DeWolf, C., McCauley, P., Sikorski, A.F., Winlove, C.P., Bailey, A.I., Kahana, E., Pinder, J.C., Gratzer, W.B., 1997. Interaction of dystrophin fragments with model membranes. Biophys. J. 72, 2599–2604.
Dos Santos Morais, R., Delalande, O., Pérez, J., Mouret, L., Bondon, A., Martel, A., Appavou, M.-S., Le Rumeur, E., Hubert, J.-F., Combet, S., 2017. Contrast-matched isotropic bicelles: a versatile tool to specifically probe the solution structure of peripheral membrane proteins using SANS. Langmuir 33, 6572–6580.
Dos Santos Morais, R., Delalande, O., Pérez, J., Mias-Lucquin, D., Lagarrigue, M., Martel, A., Molza, A.-E., Chéron, A., Raguénès-Nicol, C., Chenuel, T., Bondon, A., Appavou, M.-S., Le Rumeur, E., Combet, S., Hubert, J.-F., 2018. Human dystrophin structural changes upon binding to anionic membrane lipids. Biophys. J. 115 (7), 1231–1239.
Duan, D., 2018. Systemic AAV micro-dystrophin gene therapy for Duchenne muscular dystrophy. Mol. Ther. 26 (10), 2337–2356.
Ervasti, J.M., Campbell, K.P., 1991. Membrane organization of the dystrophin-glycoprotein complex. Cell 66 (6), 1121–1131.
Fiehn, W., Peter, J., Mead, J.F., Gan-Elepano, M., 1971. Lipids and fatty acids of sarcolemma, sarcoplasmic reticulum, and mitochondria from rat skeletal muscle. J. Biol. Chem. 246, 5617–5620.
Franke, D., Petoukhov, M.V., Konarev, P.V., Panjkovich, A., Tuukkanen, A., Mertens, H.D.T., Kikhney, A.G., Hajizadeh, N.R., Franklin, J.M., Jeffries, C.M., et al., 2017. ATSAS 2.8: a comprehensive data analysis suite for small-angle scattering from macromolecular solutions. J. Appl. Cryst. J. Appl. Crystallogr. 50, 1212–1225.
Haberkant, P., Holthuis, J.C.M., 2014. Fat & fabulous: bifunctional lipids in the spotlight. Biochim. Biophys. Acta Mol. Cell. Biol. Lipids 1841, 1022–1030.
Henderson, D.M., Lee, A., Ervasti, J.M., 2010. Disease-causing missense mutations in actin binding domain 1 of dystrophin induce thermodynamic instability and protein aggregation. PNAS 107, 9632–9637.
Henderson, D.M., Lin, A.Y., Thomas, D.D., Ervasti, J.M., 2012. The carboxy-terminal third of dystrophin enhances actin binding activity. J. Mol. Biol. 416, 414–424.
Ibraghimov-Beskrovnaya, O., Ervasti, J.M., Leveille, C.J., Slaughter, C.A., Sernett, S.W., Campbell, K.P., 1992. Primary structure of dystrophin-associated glycoproteins linking dystrophin to the extracellular matrix. Nature 355 (6362), 696–702.
Jumeau, F., Com, E., Lane, L., Duek, P., Lagarrigue, M., Lavigne, R., Guillot, L., Rondel, K., Gateau, A., Melaine, N., Guével, B., Sergeant, N., Mitchell, V., Pineau, C., 2015. Human spermatozoa as a model for detecting missing proteins in the context of the chromosome-centric human proteome project. J. Proteome Res. 14 (9), 3606–3620.
Kabsch, W., Sander, C., 1983. Dictionary of protein secondary structure: pattern recognition of hydrogen-bonded and geometrical features. Biopolymers 22, 2577–2637.
Kumar, A., Crawford, K., Close, L., Madison, M., Lorenz, J., Doetschman, T., Pawlowski, S., Duffy, J., Neumann, J., Robbins, J., et al., 1997. Rescue of cardiac alpha-actin-deficient mice by enteric smooth muscle gamma-actin. PNAS 94, 4406–4411.
Lai, Y., Thomas, G.D., Yue, Y., Yang, H.T., Li, D., Long, C., Judge, L., Bostick, B., Chamberlain, J.S., Terjung, R.L., et al., 2009. Dystrophins carrying spectrin-like repeats 16 and 17 anchor nNOS to the sarcolemma and enhance exercise performance in a mouse model of muscular dystrophy. J Clin. Invest. 119, 624–635.
Laskowski, R.A., MacArthur, M.W., Moss, D.S., Thornton, J.M., 1993. PROCHECK: a program to check the stereochemical quality of protein structures. J. Appl. Cryst. J. Appl. Crystallogr. 26, 283–291.
Lavigne, R., Becker, E., Liu, Y., Evrard, B., Lardenois, A., Primig, M., Pineau, C., 2012. Direct iterative protein profiling (DIPP) – an innovative method for large-scale protein detection applied to budding yeast mitosis. Mol. Cell. Proteomics 11 (M111), 012682.
Le, S., Yu, M., Hovan, L., Zhao, Z., Ervasti, J., Yan, J., 2018. Dystrophin as a molecular shock absorber. ACS Nano 12 (12), 12140–12148.
Legarnier, S., Raguénès-Nicol, C., Tascon, C., Rocher, C., Hardy, S., Hubert, J.F., Le Rumeur, E., 2009. Mapping of the lipid-binding and stability properties of the central rod domain of human dystrophin. J. Mol. Biol. 389 (3), 546–558.
Legrand, B., Giudice, E., Nicolas, A., Delalande, O., Le Rumeur, E., 2011. Computational study of the human dystrophin repeats: interaction properties and molecular dynamics. PLoS One 6, e23819.
Molza, A.-E., Férey, N., Czjzek, M., Le Rumeur, E., Hubert, J.-F., Tek, A., Laurent, B., Baaden, M., Delalande, O., 2014. Innovative interactive flexible docking method for multi-scale reconstruction elucidates dystrophin molecular assembly. Faraday Discuss. 169, 45–62.
Molza, A.-E., Mangat, K., Le Rumeur, E., Hubert, J.-F., Menhart, N., Delalande, O., 2015. Structural basis of neuronal nitric-oxide synthase interaction with dystrophin repeats 16 and 17. J. Biol. Chem. 290, 29531–29541.
Murakami, K., Yasunaga, T., Noguchi, T.Q.P., Gomibuchi, Y., Ngo, K.X., Uyeda, T.Q.P., Wakabayashi, T., 2010. Structural basis for actin assembly, activation of ATP hydrolysis, and delayed phosphate release. Cell 143, 275–287.
Nicolas, A., Raguénès-Nicol, C., Ben Yaou, R., Ameziane-Le Hir, S., Chéron, A., Vié, V., Claustres, M., Leturcq, F., Delalande, O., Hubert, J.-F., et al., 2015. Becker muscular dystrophy severity is linked to the structure of dystrophin. Hum. Mol. Genet. 24 (5), 1267–1279.
Prochniewicz, E., Henderson, D., Ervasti, J.M., Thomas, D.D., 2009. Dystrophin and utrophin have distinct effects on the structural dynamics of actin. PNAS 106 (19), 7822–7827.
Pyrkov, T.V., Chugunov, A.O., Krylov, N.A., Nolde, D.E., Efremov, R.G., 2009. PLATINUM: a web tool for analysis of hydrophobic/hydrophilic organization of biomolecular complexes. Bioinformatics 25 (9), 1201–1202.
Ramaswamy, K.S., Palmer, M.L., van der Meulen, J.H., Renoux, A., Kostrominova, T.Y., Michele, D.E., Faulkner, J.A., 2011. Lateral transmission of force is impaired in skeletal muscles of dystrophic mice and very old rats. J. Physiol. 589, 1195–1208.
Ramos, J.N., Hollinger, K., Bengtsson, N.E., Allen, J.M., Hauschka, S.D., Chamberlain, J.S., 2019. Development of novel micro-dystropins with enhanced functionality. Mol. Ther. 27 (3), 623–635.
Rybakova, I.N., Amann, K.J., Ervasti, J.M., 1996. A new model for the interaction of dystrophin with F-actin. J. Cell Biol. 135, 661–672.
Rybakova, I.N., Patel, J.R., Davies, K.E., Yurchenco, P.D., Ervasti, J.M., 2002. Utrophin binds laterally along actin filaments and can couple costameric actin with sarcolemma when overexpressed in dystrophin-deficient muscle. Mol. Biol. Cell 13 (5), 1512–1521.
Rybakova, I.N., Humston, J.L., Sonnemann, K.J., Ervasti, J.M., 2006. Dystrophin and utrophin bind actin through distinct modes of contact. J. Biol. Chem. 281 (15), 9996–10001.
Sarkis, J., Hubert, J.-F., Legrand, B., Robert, E., Chéron, A., Jardin, J., Hitti, E., Le Rumeur, E., Vié, V., 2011. Spectrin-like repeats 11–15 of human dystrophin show adaptations to a lipidic environment. J. Biol. Chem. 286, 30481–30491.
Sarkis, J., Vié, V., Winder, S.J., Renault, A., Rumeur, E.L., Hubert, J.-F., 2013. Resisting sarcolemmal rupture: dystrophin repeats increase membrane-actin stiffness. FASEB J. 27, 359–367.
Schneider, S., Saladin, A., Fiorucci, S., Prévost, C., Zacharias, M., 2012. ATTRACT and PTools: open source programs for protein-protein docking. Meth. Mol. Biol. 819, 221–232.
Singh, S.M., Mallela, K.M.G., 2012. The N-terminal actin-binding tandem calponin-homology (CH) domain of dystrophin is in a closed conformation in solution and when bound to F-actin. Biophys. J. 103 (9), 1970–1978.
Singh, S.M., Molas, J.F., Kongari, N., Bandi, S., Armstrong, G.S., Winder, S.J., Mallela, K.M.G., 2012. Thermodynamic stability, unfolding kinetics, and aggregation of the N-terminal actin-binding domains of utrophin and dystrophin. Proteins 80 (5), 1377–1392.
Sonnemann, K.J., Fitzsimons, D.P., Patel, J.R., Liu, Y., Schneider, M.F., Moss, R.L., Ervasti, J.M., 2006. Cytoplasmic gamma-actin is not required for skeletal muscle development but its absence leads to a progressive myopathy. Dev. Cell 11, 387–397.
Stark, A.E., 2015. Determinants of the incidence of Duchenne muscular dystrophy. Ann. Transl. Med. 3 (19), 287.
Touw, W.G., Baakman, C., Black, J., te Beek, T.A.H., Krieger, E., Joosten, R.P., Vriend, G., 2015. A series of PDB-related databanks for everyday needs. Nucl. Acids Res. 43, D364–D368.
Valentini, E., Kikhney, A.G., Previtali, G., Jeffries, C.M., Svergun, D.I., 2015. SASBDB, a repository for biological small-angle scattering data. Nucl. Acids Res. 43, D357–D363.
Vié, V., Legardinier, S., Chieze, L., Le Bihan, O., Qin, Y., Sarkis, J., Hubert, J.-F., Renault, A., Desbat, B., Le Rumeur, E., 2010. Specific anchoring modes of two distinct dystrophin rod sub-domains interacting in phospholipid Langmuir films studied by atomic force microscopy and PM-IRRAS. Biochim. Biophys. Acta (BBA) – Biomembr. 1798, 1503–1511.
Wein, N., Alfano, L., Flanigan, K.M., 2015. Genetics and emerging treatments for Duchenne and Becker muscular dystrophy. Pediatr. Clin. North Ama. 62 (3), 723–742.
Winder, S.J., Hemmings, L., Maciver, S.K., Bolton, S.J., Tinsley, J.M., Davies, K.E., Critchley, D.R., Kendrick-Jones, J., 1995a. Utrophin actin binding domain: analysis of actin binding and cellular targeting. J. Cell Sci. 108 (Pt 1), 63–71.
Winder, S.J., Gibson, T.J., Kendrick-Jones, J., 1995b. Dystrophin and utrophin: the missing links!. FEBS Lett. 369, 27–33.
Yokota, T., Duddy, W., Echigoya, Y., Kolski, H., 2012. Exon skipping for nonsense mutations in Duchenne muscular dystrophy: too many mutations, too few patients? Expert Opin. Biol. Ther. 12, 1141–1152.
Zhao, J., Kodippili, K., Yue, Y., Hakim, C.H., Wasala, L., Pan, X., Zhang, K., Yang, N.N., Duan, D., Lai, Y., 2016. Dystrophin contains multiple independent membrane-binding domains. Hum. Mol. Genet. 25, 3647–3653.